

Supporting Information

Long-Range Exciton Diffusion in a Non-Fullerene Acceptor: Approaching the Incoherent Limit

Paul A. Hume*,†,‡, Wanting Jiao,‡ Justin M. Hodgkiss†,‡

†MacDiarmid Institute for Advanced Materials and Nanotechnology, Wellington 6010, New Zealand

‡School of Chemical and Physical Sciences, Victoria University of Wellington, Wellington 6010, New Zealand

Corresponding Author: [*paul.hume@vuw.ac.nz](mailto:paul.hume@vuw.ac.nz)

Contents

S.1.	Franck-Condon Integrals	S2-S3
S.2.	Comparison of Short-Range Coupling Values	S3
S.3.	Geometries of Crystal Pairs with Short-Range Contacts	S4
S.4.	Spatiotemporal ATC Coupling Distributions for Close Contacts	S5-S6
S.5.	Spatiotemporal Molecular Orbital Overlap Distributions for Close Contacts	S6
S.6.	Accessible Hopping Site Distributions	S7-S8
S.7.	Sum-Over-Rates Diffusivity Distributions for Crystal Position 2	S9
S.8.	Reported Diffusion Coefficients for Common Solution-Processed OPV Materials	S9
S.9.	References	S10

S.1. Franck-Condon Integrals

The Huang-Rhys parameters for each of the ground state normal modes were calculated by projection of the difference between the optimised excited state geometry and the ground state (in mass-weighted coordinates) onto the normal modes of the ground state and calculating the associated Huang-Rhys parameters (Figure S1).

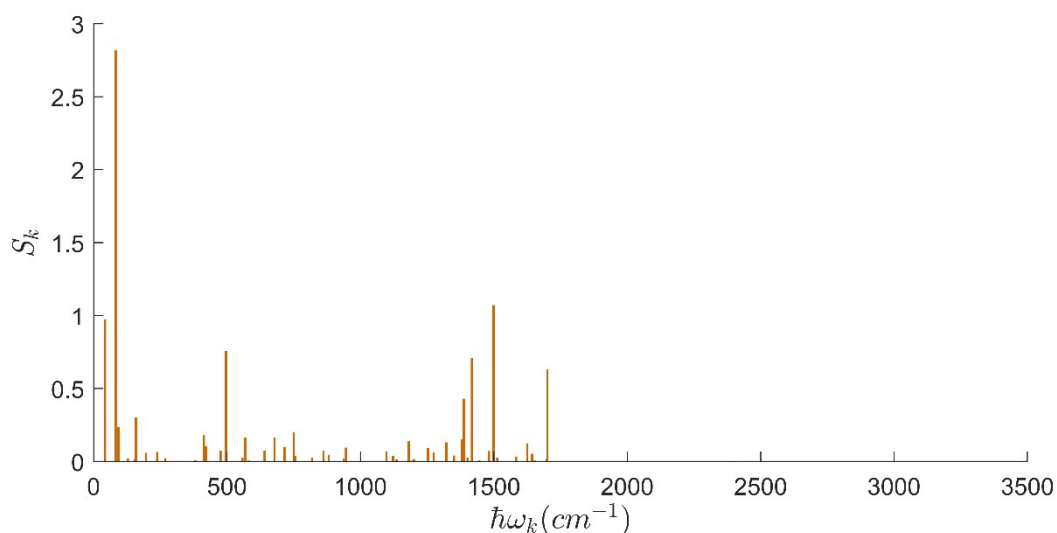


Figure S1. Calculated Huang-Rhys parameters S_k .

The effective vibrational mode was selected according to Equations S1-S4, by identifying four high-frequency modes coupled to photoexcitation (1388, 1418, 1499, and 1701 cm^{-1}). The frequency of ω^{eff} was chosen to approximately coincide with the weighted mean of these vibrations (1500 cm^{-1}), and S^{eff} was set equal to 0.91, to preserve the sum of quantum-mechanical contributions to the reorganisation energy from modes at 1350-1750 cm^{-1} . When estimating S^{eff} , the λ_k for dimeric systems

were approximated as $2\left(\frac{k_i}{2}\Delta Q_i^2\right)$, where k_i is the ground state force constant for vibrational mode i , and $\Delta Q_i = Q_i^{ES} - Q_i^{GS}$ is the normal mode displacement associated with moving from the optimal ground state geometry to that of the excited state, for a single molecule. This approach enables the use of ground state vibrational modes, in line with previous work.^{S1}

$$\lambda = \sum_i \lambda_i \quad (S1) \quad \lambda_i = \frac{k_i}{2} \Delta Q_i^2 \quad (S2)$$

$$S_i = \frac{\lambda_i}{\hbar\omega_i} \quad (S3) \quad \lambda_q = S^{eff} \hbar\omega^{eff} \quad (S4)$$

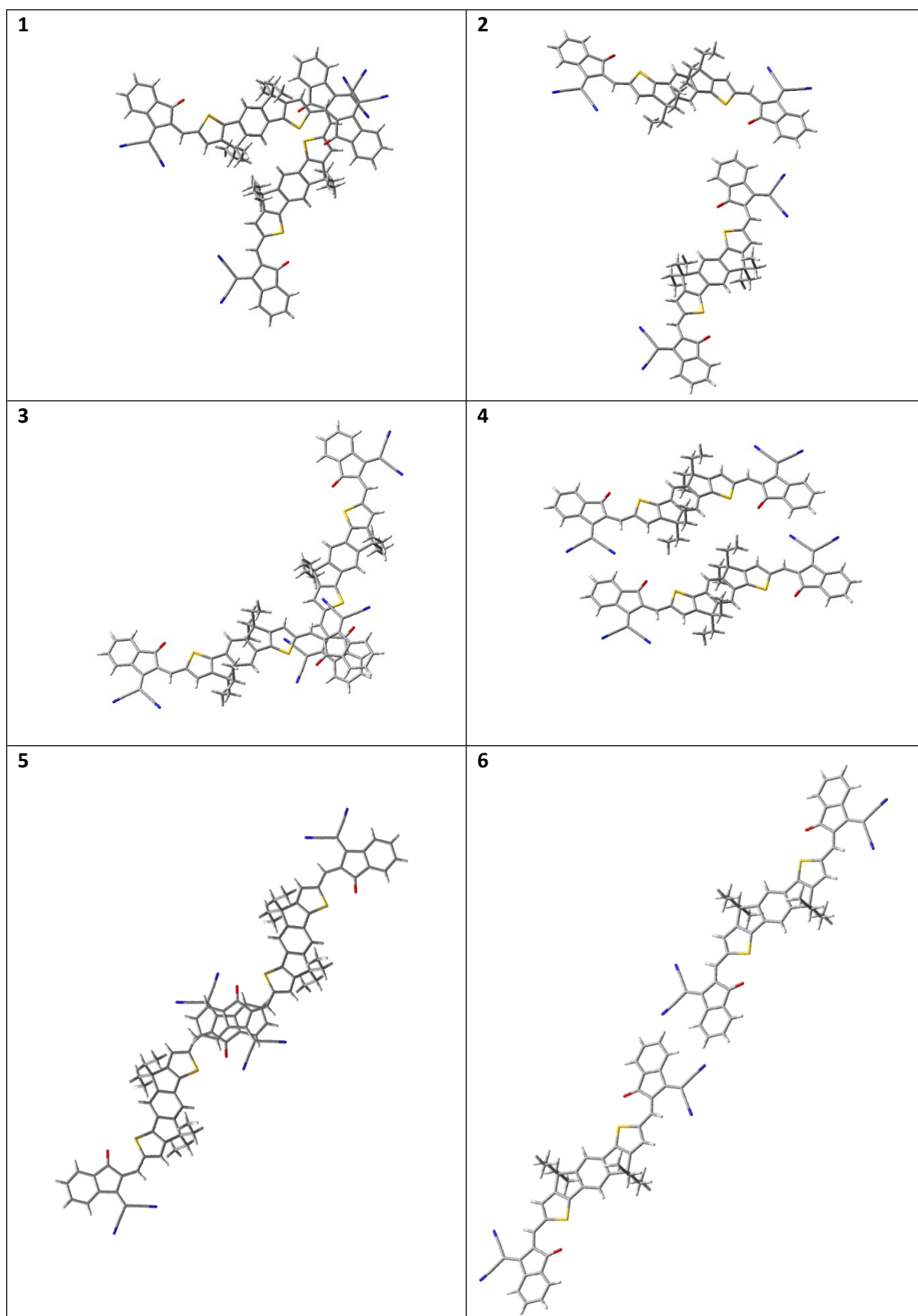
S^{eff} is then used to calculate the Franck-Condon integrals according to Equation S5.^{S2}

$$|\langle \chi_w | \chi_{w'} \rangle|^2 = e^{-S^{eff}/2} \sum_{u=0}^w \sum_{u'=0}^{w'} \frac{(-1)^{u'} (\sqrt{S^{eff}})^{u+u'}}{u!u'!} \sqrt{\frac{w!w'!}{(w-u)!(w'-u)!}} \delta_{w-u, w'-u'} \quad (S5)$$

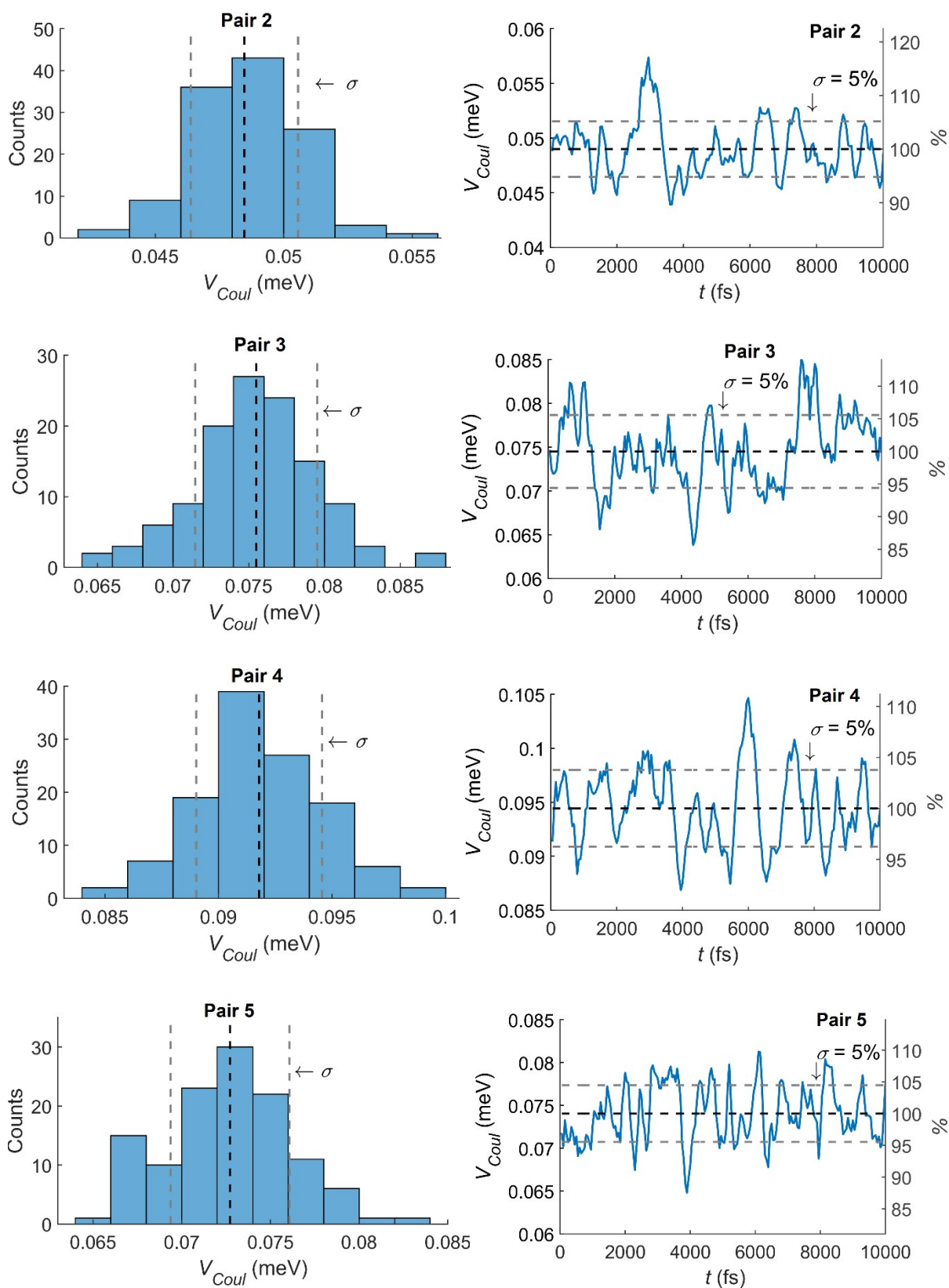
S.2. Comparison of Short-Range Coupling Values (meV)

Pair	Projective Coupling ($\epsilon_{PCM} = 5$)	Projective Coupling (Vacuum)	FED (Vacuum)
1	63.4	74.3	72.1
2	28.5	39.7	40.1
3	52.6	63.0	63.0
4	52.4	73.0	72.2
5	48.3	58.0	60.1
6	31.4	44.3	44.6

S.3. Geometries of Crystal Pairs with Short-Range Contacts



S.4. Spatiotemporal ATC Coupling Distributions for Close Contacts



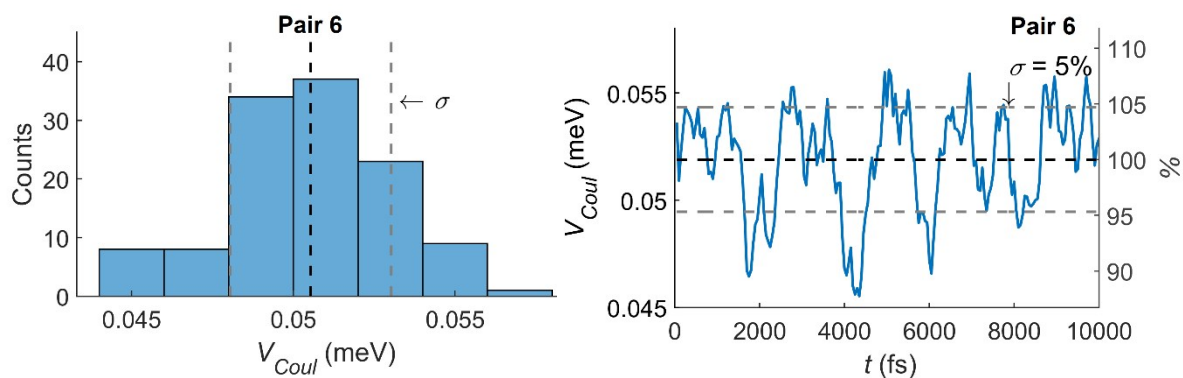


Figure S2. Spatial and temporal variation in ATC electronic couplings for “close-contact” molecular pairs extracted from the MD trajectory that were symmetry-equivalent prior to the introduction of thermal motion.

S.5. Spatiotemporal Molecular Orbital Overlap Distributions for Close Contacts

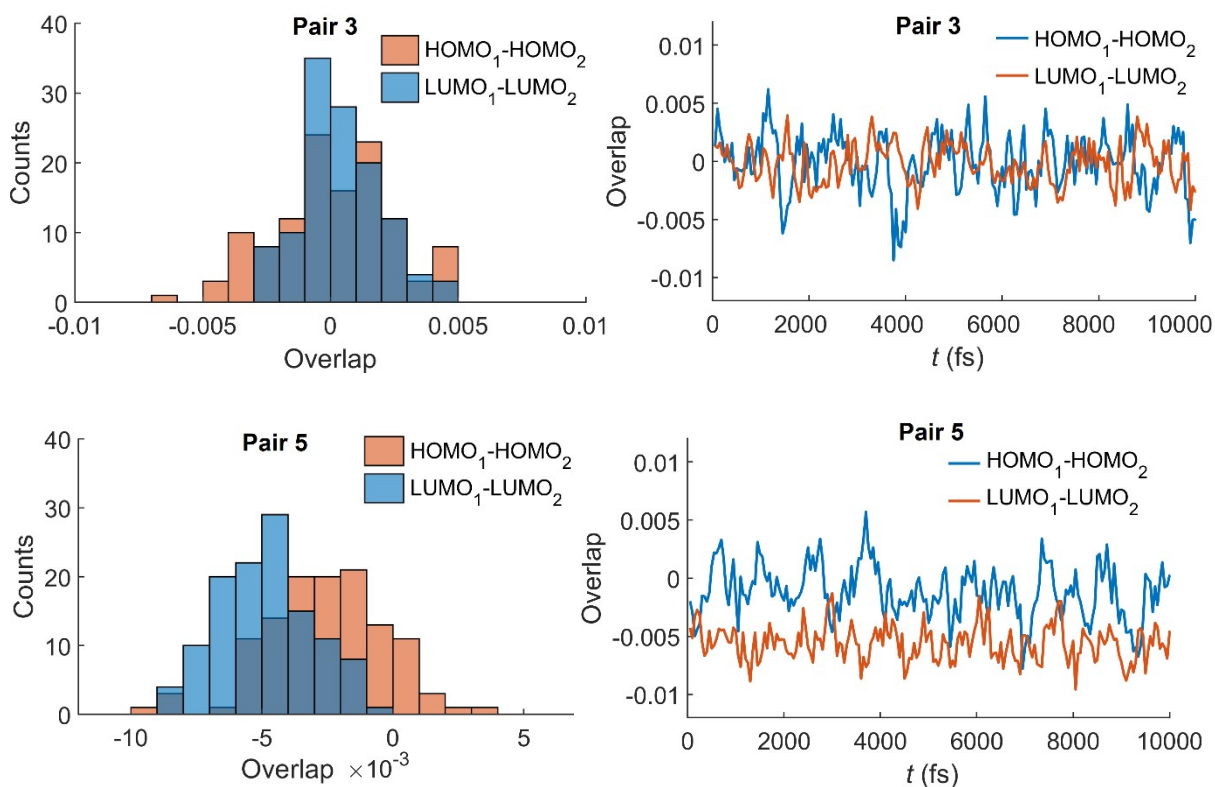


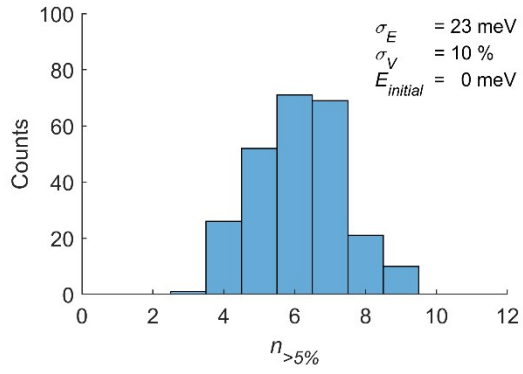
Figure S3. Spatial and temporal variation in selected MO overlaps for π -stacked molecular pairs extracted from the MD trajectory.

S.6. Accessible Hopping Site Distributions

As mentioned in the main text, Equation 5 is invalid when a small number of hopping sites only permits energy transfer to other members of the set. Equation 5 only considers a single hop, and is therefore unable to account for the fact that hops between molecules in the trap region or grain can remain fast (and therefore result in a large predicted D), but the macroscopic diffusion length is limited by the boundaries of the trap region (the error associated with Equation 5 was also quantified in the main text by comparison with Monte-Carlo simulations). Despite this limitation, Equation 5 remains a useful tool to predict diffusion coefficients, because the combination of low disorder, 3-dimensional transport, and significant excitonic couplings to multiple acceptor molecules means that such regions are expected to be rare in IDIC. To examine this idea, we provide distributions of the number of neighbouring molecules with a transfer probability of >5% for different levels of energetic disorder, and different energies of the initial hopping site.

Figure S4 shows that for $\sigma_E = 23$ meV and a sample size of 250, the minimum number of available hopping sites is 3, and most have at least 6 available sites, for all initial site energies examined. When $\sigma_E = 50$ meV (Figure S5), sites which only have one significant acceptor site are more common, especially below the thermalisation energy, but multiple transfer channels generally still remain.

Position 1



Position 2

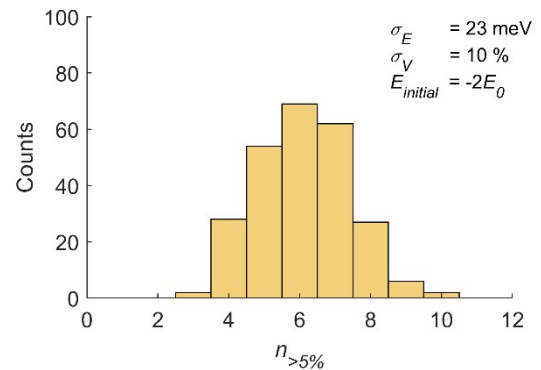
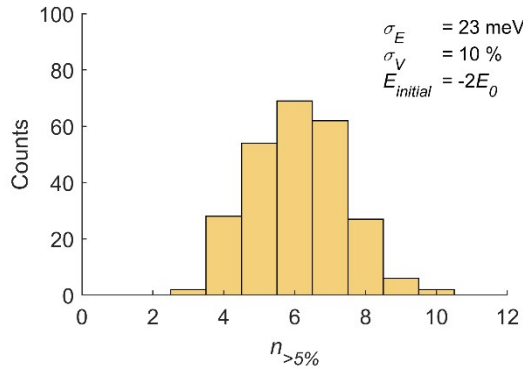
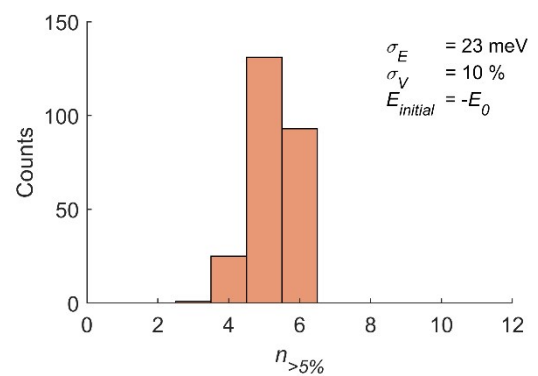
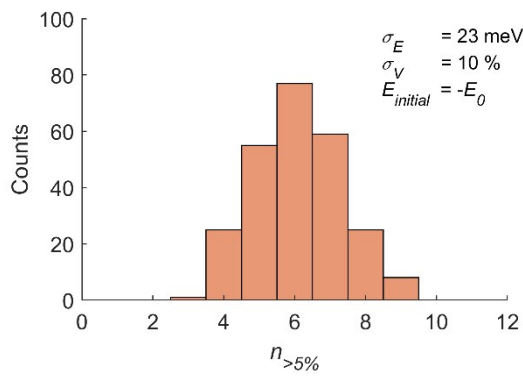
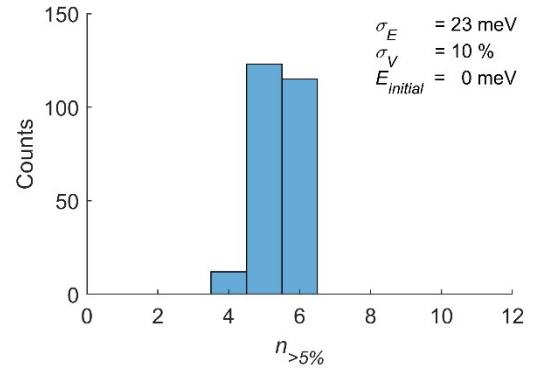


Figure S4. Number of hopping sites with greater than 5% transfer probability for positions 1 and 2. E_0 is the magnitude of the thermalisation energy, $\sigma_E^2/k_B T$, where $\sigma_E = 23 \text{ meV}$, $\sigma_V = 10\%$, k_B is the Boltzmann constant, and $T = 298 \text{ K}$.

S.7. Sum-Over-Rates Diffusivity Distributions for Crystal Position 2

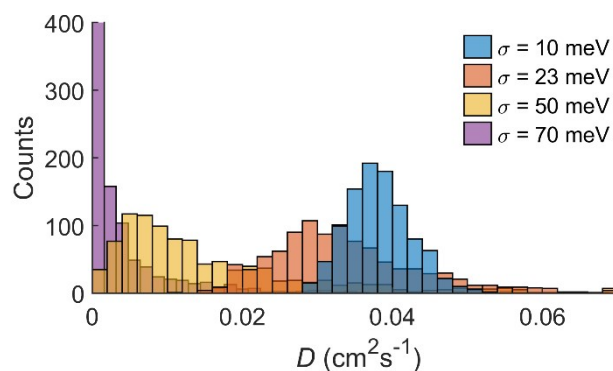


Figure S5. Sum-over-rates diffusion coefficients for IDIC at different levels of energetic disorder, for an exciton initially located at unit cell position 2.

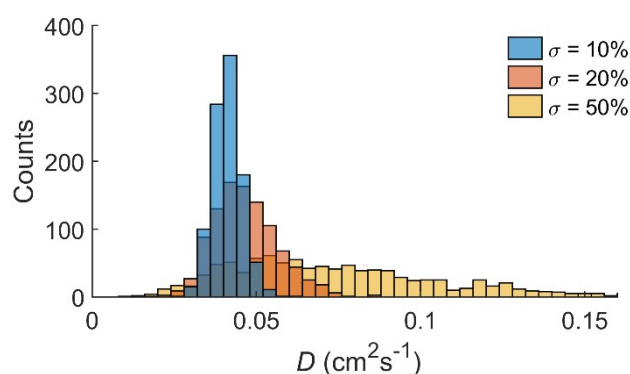


Figure S6. Sum-over-rates diffusion coefficients for IDIC with different coupling fluctuation magnitudes for a exciton initially located at unit cell position 2.

S.8. Reported Diffusion Coefficients for Common Solution-Processed OPV Materials

Material	D (cm^2/s)	Reference
P3HT	0.0018	S3
PC_{71}BM	0.00016	S4
PCPDTBT	0.003	S5
PPV Derivatives	0.0003-0.003	S6

For a more comprehensive tabulation of experimentally-measured diffusion coefficients/lengths, we refer the reader to the Supporting Information of Reference S7.

S.9. References

- S1. J. Aragó and A. Troisi, *Adv. Funct. Mater.*, 2016, **26**, 2316.
- S2. R. P. Fornari, J. Aragó and A. Troisi, *J. Chem. Phys.*, 2015, **142**, 184105.
- S3. P. E. Shaw, A. Ruseckas and I. D. W. Samuel, *Adv. Mater.*, 2008, **20**, 3516.
- S4. G. J. Hedley, A. J. Ward, A. Alekseev, C. T. Howells, E. R. Martins, L. A. Serrano, G. Cooke, A. Ruseckas and I. D. Samuel, *Nat. Commun.*, 2013, **4**, 2867.
- S5. O. V. Mikhnenko, M. Kuik, J. Lin, N. van der Kaap, T. Q. Nguyen and P. W. Blom, *Adv. Mater.*, 2014, **26**, 1912.
- S6. D. E. Markov, C. Tanase, P. W. M. Blom and J. Wildeman, *Phys. Rev. B*, 2005, **72**, 045217.
- S7. Y. Firdaus, V. M. Le Corre, S. Karuthedath, W. Liu, A. Markina, W. Huang, S. Chattopadhyay, M. M. Nahid, M. I. Nugraha, Y. Lin, A. Seitkhan, A. Basu, W. Zhang, I. McCulloch, H. Ade, J. Labram, F. Laquai, D. Andrienko, L. J. A. Koster and T. D. Anthopoulos, *Nat. Commun.*, 2020, **11**, 5220.